iScience

CellPress
OPEN ACCESS

Article

Pathway and directional specificity of Hebbian plasticity in the cortical visual motion processing network

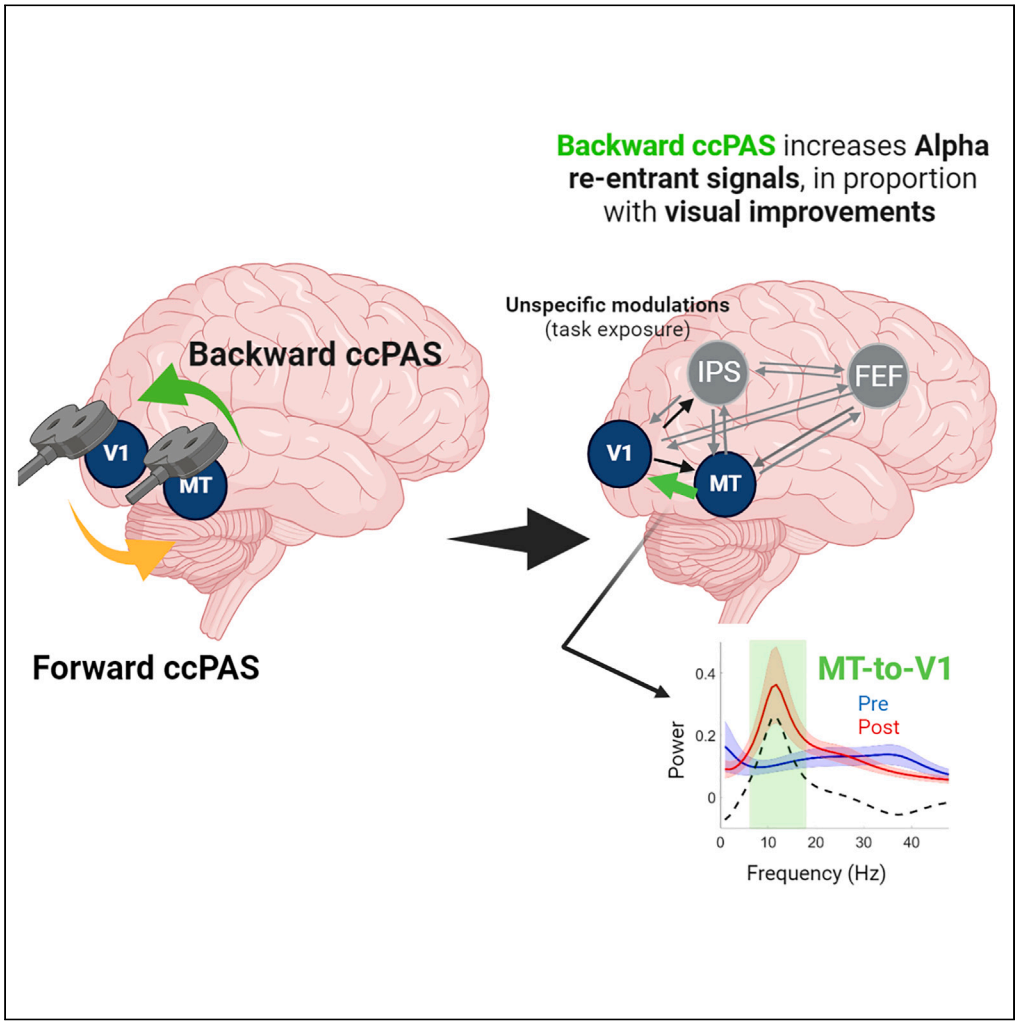

Michele Bevilacqua, Krystel R. Huxlin, Friedhelm C. Hummel, Estelle Raffin

estelle.raffin@epfl.ch

Highlights

Applying Hebbian rules of associative plasticity increases backward alpha MT-to-V1 inputs

Enhancing backward projections scaled with motion discrimination performances

Stimulating in the reverse direction did not change forward connectivity or performances

Bevilacqua et al., iScience *26*, 107064
July 21, 2023
https://doi.org/10.1016/j.isci.2023.107064

iScience

CellPress
OPEN ACCESS

Article

Pathway and directional specificity of Hebbian plasticity in the cortical visual motion processing network

Michele Bevilacqua,[1,2] Krystel R. Huxlin,[3] Friedhelm C. Hummel,[1,2,4,5] and Estelle Raffin[1,2,5,6,*]

SUMMARY

Cortico-cortical paired associative stimulation (ccPAS), which repeatedly pairs single-pulse transcranial magnetic stimulation (TMS) over two distant brain regions, is thought to modulate synaptic plasticity. We explored its spatial selectivity (pathway and direction specificity) and its nature (oscillatory signature and perceptual consequences) when applied along the ascending (*Forward*) and descending (*Backward*) motion discrimination pathway. We found unspecific connectivity increases in bottom-up inputs in the low gamma band, probably reflecting visual task exposure. A clear distinction in information transfer occurred in the re-entrant alpha signals, which were only modulated by Backward-ccPAS, and predictive of visual improvements in healthy participants. These results suggest a causal involvement of the re-entrant MT-to-V1 low-frequency inputs in motion discrimination and integration in healthy participants. Modulating re-entrant input activity could provide single-subject prediction scenarios for visual recovery. Visual recovery might indeed partly rely on these residual inputs projecting to spared V1 neurons.

INTRODUCTION

Visual processing represents a massive computational task for the brain, requiring highly organized and efficient neural systems to achieve accurate perception. In primates, approximately 55% of the cortex contributes to visual processing (compared to 11% for somatosensory processing or 3% for auditory processing).[1] Multiple components of the visual system receive, relay, and ultimately process visual information. These structures include the eye, retina, optic nerves, chiasm, tracts, lateral geniculate nucleus (LGN) of the thalamus, the superior colliculus, optic radiations, the primary visual (or striate, V1) cortex, and multiple extrastriate visual cortical areas. Information processing relies not only on forward connections from lower to higher level visual areas but also on connections that transfer information in the opposite direction. These backward connections, which are much more numerous than the forward inputs coming from the LGN[2] and from the lower level visual areas V1 and V2, are thought to adjust, regulate, and improve the processing of incoming stimuli.[3–5] Therefore, neural responses in V1 do not mirror retinal inputs precisely, but are modified by higher inputs to support a coherent perceptual interpretation.

One of the most studied cortical visual processing pathways is the one specialized in decoding motion stimuli.[6] The very early stage involves the primary visual cortex (V1). Early single-unit recordings in macaque and cats showed that a subset of cells in V1 is highly direction selective.[7–9] These direction-sensitive cells then project onto the medial temporal area (MT[10]), where all neurons appear to be directionally selective,[6,11,12] with activity well-correlated with behavioral performance on motion tasks.[13] The information reaches the higher motion areas (MT, MST, and V6) also through indirect projection through V2 and V3a areas.[14,15] More precisely, MT neurons are capable of coding the direction and speed of the image motion.[16–19] As such, lesions to primate V1[20–22] or MT[22–25] will both cause deficits in visual motion perception. Transcranial magnetic stimulation (TMS) studies in humans provide further evidence supporting the role of both areas in motion discrimination.[26,27] The majority of humans and macaques' studies have concentrated on the capacity of MT cells to register motion in the fronto-parallel plane and on their directional properties and speed preferences.[9,19,24,28] In this regard, Ruzzoli and colleagues[29] studied the effect of a TMS perturbation on the shape of the psychometric function in a visual motion discrimination task, showing a decrement in motion discrimination performance when TMS was applied over MT concomitantly with the motion

[1]Defitech Chair in Clinical Neuroengineering, Neuro-X Institute (NRX) and Brain Mind Institute, EPFL, Geneva, Switzerland

[2]Defitech Chair in Clinical Neuroengineering, Neuro-X Institute (NRX) and Brain Mind Institute, Clinique Romande de Readaptation (CRR), EPFL Valais, Sion, Switzerland

[3]The Flaum Eye Institute and Center for Visual Science, University of Rochester, Rochester, NY, USA

[4]Clinical Neuroscience, University of Geneva Medical School, Geneva, Switzerland

[5]These authors contributed equally

[6]Lead contact

*Correspondence: estelle.raffin@epfl.ch

https://doi.org/10.1016/j.isci.2023.107064

stimulus. Furthermore, the authors found that TMS specifically affected the perceptual ability to discriminate motion direction rather than higher cognitive processes such as perceptual consciousness, decision-making, or response selection and execution.

The interaction and synchronization between visual areas have been previously modeled. One of the first computational models that simulated dynamic integration in the visual system and the pivotal role of backward connections between visual areas in motion perception processing was proposed by Tononi et al.[30] The model suggested that re-entrant connections in the visual cortex are mostly integrative, i.e., they facilitate the coordination of neuronal firing in anatomically and functionally segregated cortical areas. Thus, neural responses related to the detection of motion coherence may depend on re-entrant projections from area MT to area V1, which have been found to be mostly excitatory.[31] The timing of the backward inputs from MT to V1 has been studied in humans using visual masking stimuli, visually evoked potentials,[32] or by TMS perturbation.[34–36] TMS studies targeting MT have consistently shown two periods of disruption, suggestive of forward/backward processes.[34] Furthermore, paired-pulse TMS protocols can estimate the time delay for information transfer along the pathway. For instance, Pascual-Leone and Walsh[35] showed significant impairments of coherent perceptual interpretation of motion when an MT pulse was given 10 to 30 ms before a V1 pulse. Importantly, this processing channel possesses characteristic oscillatory activity that has been linked to the transfer of specific stimulus features or endogenous variables within the pathway. Indeed, backward projections have been found to be mediated by low-frequency alpha/beta oscillations while forward connections are thought to be supported by high-frequency gamma oscillations, in both monkeys[37,38] and humans.[39]

A more direct approach to non-invasively test the role of backward projections in motion discrimination is to causally manipulate the synaptic strength of top-down MT-to-V1 connections. This is possible through the use of cortico-cortical paired associative stimulation (ccPAS),[40–45] an approach that relies on Hebbian Learning theory, which states that the pairing of subthreshold synaptic stimulation and action potential trains can induce long-term potentiation (LTP).[46] More precisely, the induction of LTP requires activation of the presynaptic input milliseconds before the backpropagating action potential in the postsynaptic dendrite. The first human applications performed by Stefan et al.[47] showed that low-frequency TMS over the primary motor cortex following peripheral stimulation of the median nerve induced plastic changes in the human motor system when using timings relevant for spike-timing-dependent plasticity.[48]

This concept has been applied to cortico-cortical connections—e.g., between frontal and parietal areas,[49] or between the cerebellum and M1.[50] ccPAS has also been applied to the V1-MT pathway.[51] These authors compared different versions of ccPAS between V1 and MT in healthy subjects and found that only ccPAS targeting the re-entrant connection from MT to V1 with an optimal time delay of 20 ms was effective in boosting motion discrimination capacities up to 90 min.

In the present study, we applied ccPAS to the V1-MT pathway to compare the effects of enhancing forward or ascending versus backward or descending projections on motion discrimination and visual network activity (Forward-ccPAS versus Backward-ccPAS). We used electroencephalography (EEG), and spectral Granger causality-based network analyses to investigate pathway specificity and directional specificity of ccPAS, as well as the spectral content of the induced changes. The combination of spectral Granger causality and single-pulse TMS over V1 and MT allowed us to distinguish output connectivity from re-entrant connectivity.[52] In line with the prior study by Romei et al.,[51] we hypothesized that enhancing backward projections would induce larger behavioral improvements and would be associated with a specific increase in connectivity restricted to the re-entrant backward MT to V1 inputs, especially in the alpha band. Conversely, we hypothesized that enhancing forward inputs would induce non-specific changes in bottom-up direct output connections, not necessarily relevant for motion perception.

RESULTS

16 healthy subjects participated in a double-blinded and cross-over study, involving two sessions of 3 h each, only differing by the type of ccPAS intervention applied to the participants (Forward-ccPAS, strengthening V1-to-MT connexion or Backward-ccPAS, strengthening MT-to-V1 connexion, Figure 1A). The two sessions were performed at least one month apart and the order was randomized and counterbalanced between participants. Each session comprised a familiarization phase to ensure that subjects understood the visual discrimination task and reached stable performance. After EEG cap preparation, TMS sites and

CellPress
OPEN ACCESS

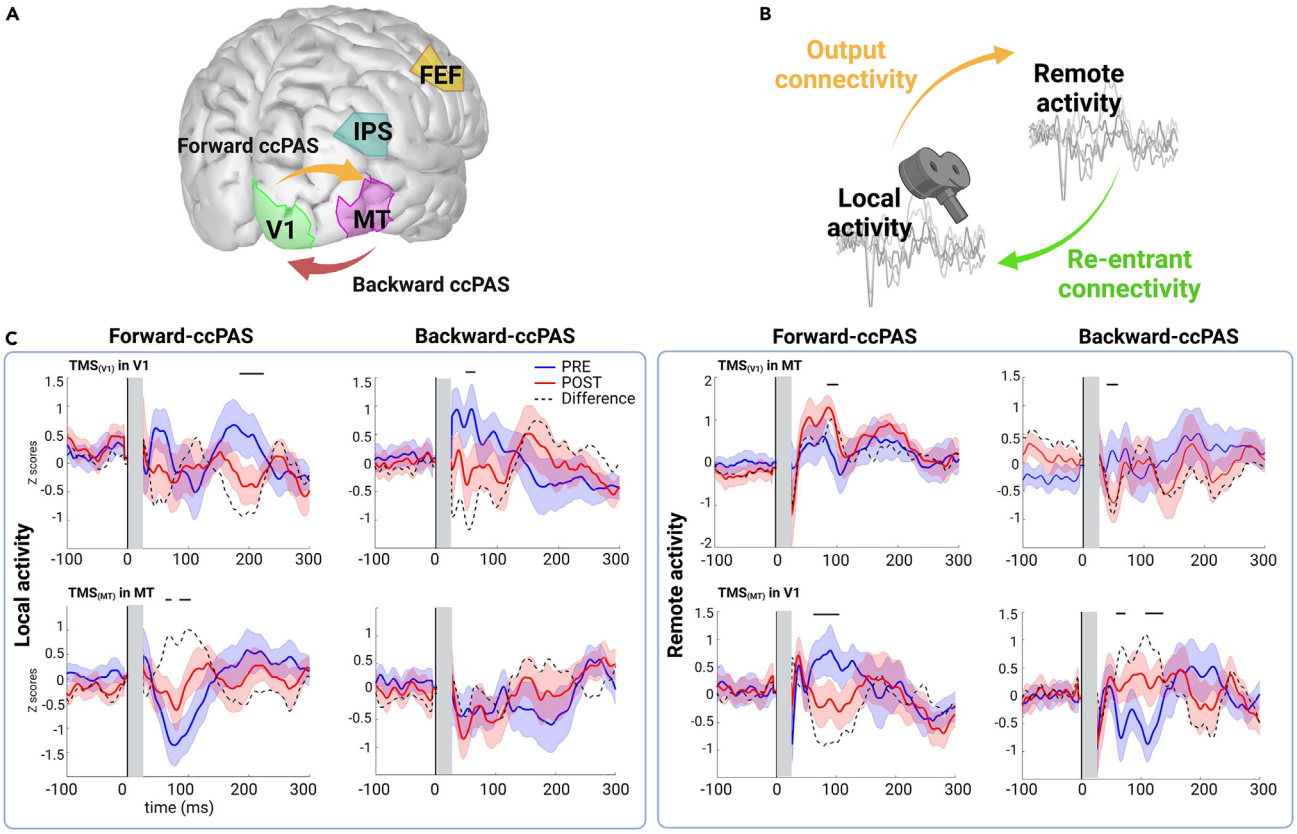

Figure 1. Local and remote source activity in the regions of interest

(A) Illustration of the Backward- and Forward-ccPAS interventions as well as the four regions of interest.

(B) Illustration of the main EEG outcomes, local and remote source activity (LSA and RSA), output and re-entrant Granger causality connectivity between V1 and MT.

(C) Right panel: LSA profiles in response to single-pulse TMS over V1 (top) and TMS over MT (bottom) for Forward-ccPAS (left) and Backward-ccPAS (right). Left panel: RSA profiles in response to single-pulse TMS over V1 (top) and TMS over MT (bottom) for Forward-ccPAS (left) and Backward-ccPAS (right). The blue and red lines and shaded areas represent mean and standard error of the mean of LSA power z-scored against baseline. Black bars indicate periods of significant difference between PRE and POST using non-parametric, cluster-based, corrected, permutation tests.

intensities were defined (see method details). Task performances were extracted at baseline, and after ccPAS using normalized direction range (NDR) thresholds as classically used in signal theory.[21] EEG responses to single-pulse TMS over V1 and MT were also recorded at baseline and after ccPAS. During the whole experiment, the participants sat on a chair, with the head leaning on the chinrest, in front of a computer screen, centered 47 cm far from the eyes. The two sessions were equally rated in terms of discomfort and sensations. One participant dropped out, resulting in 16 datasets for Forward-ccPAS and 15 datasets for Backward-ccPAS.

Local and remote source activity from single-pulse TMS

We used the local EEG source activity to measure the local responses to single-pulse TMS and the remote EEG source activity to infer about long-range effects (Figure 1B). On the local source activity, we observed a decrease over V1 (from 15 to 100 ms), only significant for the Backward-ccPAS (Figure 1C, left column). In contrast, Forward-ccPAS induced an increase in local MT activity (30–150 ms). Note that a significant decrease was also found in the late components (>200 ms) in local V1 after Forward-ccPAS. When source activity was extracted from the opposite area, Forward-ccPAS decreased remote MT activity in response to TMS over V1 (from 45 to 100 ms) (Figure 1C, second box) while Backward-ccPAS showed the opposite effects (from 45 to 60 ms and from 110 to 130 ms). When TMS was applied to V1, Forward-ccPAS showed a transient decrease in MT (80–100 ms) while Backward-ccPAS showed a decrease (60–75 ms).

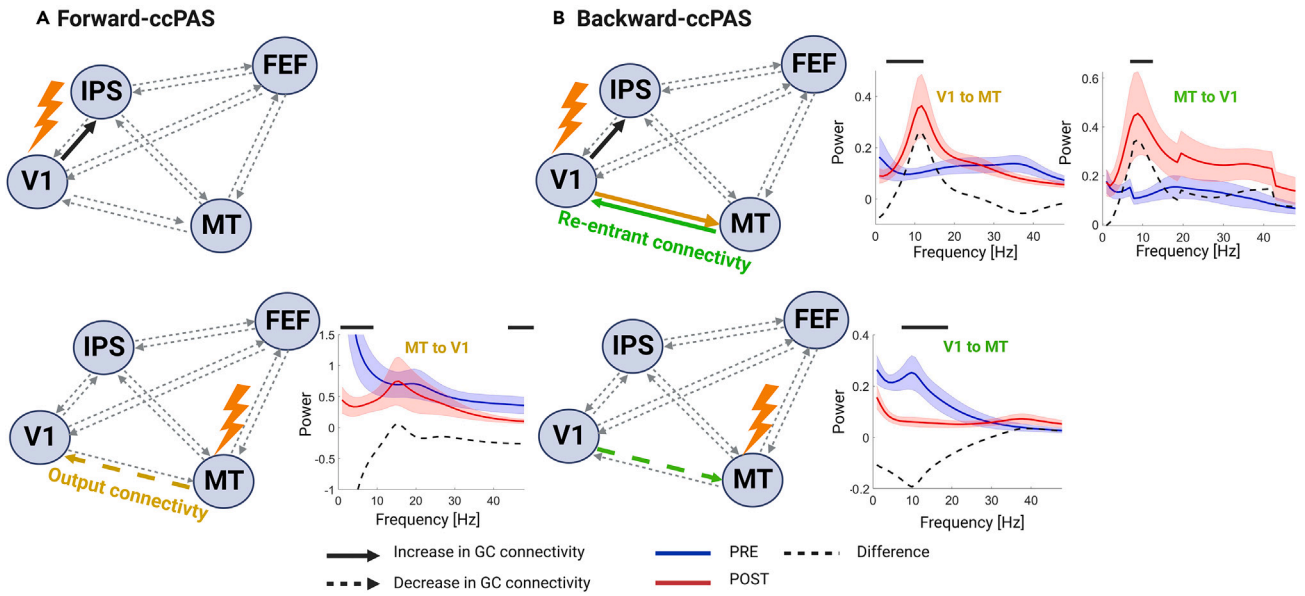

Figure 2. Changes in functional connectivity patterns

(A) Spectral Granger causality of the visual network after single-pulse TMS on V1 (upper row) and MT (bottom row) for Forward-ccPAS.

(B) Spectral Granger causality of the visual network after single-pulse TMS on V1 (upper row) and MT (bottom row) for Backward-ccPAS condition. Spectral plots displaying significant changes in Granger causality in the frequency domain are displayed for the V1-MT pathway on the right. The blue and red lines and shaded areas represent the mean and the standard error of the mean PRE and POST ccPAS, respectively. Black bars indicate periods of significant differences between PRE and POST using non-parametric, cluster-based, corrected, permutation tests.

Connectivity changes in response to single-pulse TMS

We explored effective connectivity at different frequency ranges using spectral Granger causality, which reflects directed interareal influence[53] in a broader visual network known to be involved in motion direction discrimination (Pascual-Leone and Walsh, 2001). Combining single-pulse TMS with Granger causality, we dissociated *Output Connectivity* from *Re-entrant Connectivity* (Figure 1B). The results showed that Forward-ccPAS (Figure 2, left column) caused a significant increase in the bottom-up V1-to-intraparietal sulcus (IPS) connectivity in the gamma band (35–45 Hz), when V1 was stimulated. When MT was stimulated, the V1-to-IPS connectivity was also upregulated in the theta-alpha band (5–12 Hz), while the top-down MT-to-V1 inputs were significantly inhibited in the alpha and gamma bands.

Backward-ccPAS (Figure 2, right column) also significantly increased direct bottom-up inputs (V1-to-MT and V1-to-IPS) in the alpha band when V1 was stimulated. Interestingly, the re-entrant MT-to-V1 pathway was also increased in the alpha range (MT-to-V1). When MT was stimulated, the re-entrant V1-to-MT inputs significantly decreased in the alpha band.

Behavioral results

To examine whether the changes in EEG activity and interareal connectivity translated into perceptual changes, we used a 2-alternative, forced-choice, left-right, global direction discrimination and integration task, as previously described.[21,54–57] Subjects were asked to discriminate the left–right direction of motion of random-dot stimuli centered at Cartesian coordinates [-5°, 5°] (i.e., the bottom left quadrant of the visual field, relative to central fixation, see Figure 3E). Self-confidence was rated (low/medium/high) after each trial. Auditory feedback indicated whether the response was correct or incorrect. To measure changes in performance, we computed direction range thresholds by fitting a Weibull function to the percentage correct performance at each stimulus level and computed the stimulus value (i.e., direction range), resulting in 75% correct performance. Direction range thresholds were then normalized by the maximum range (360) to produce the normalized direction ratio (NDR)[20] (see the STAR Methods section for more details).

A mixed ANOVA on the NDR values showed a main effect of Time ($F_{(1,11)} = 13.3$, $p = 0.004$) and a significant ccPAS type x Time ($F_{(1,11)} = 5.37$, $p = 0.04$). The post-hoc comparisons showed that the pre-post difference

CellPress
OPEN ACCESS

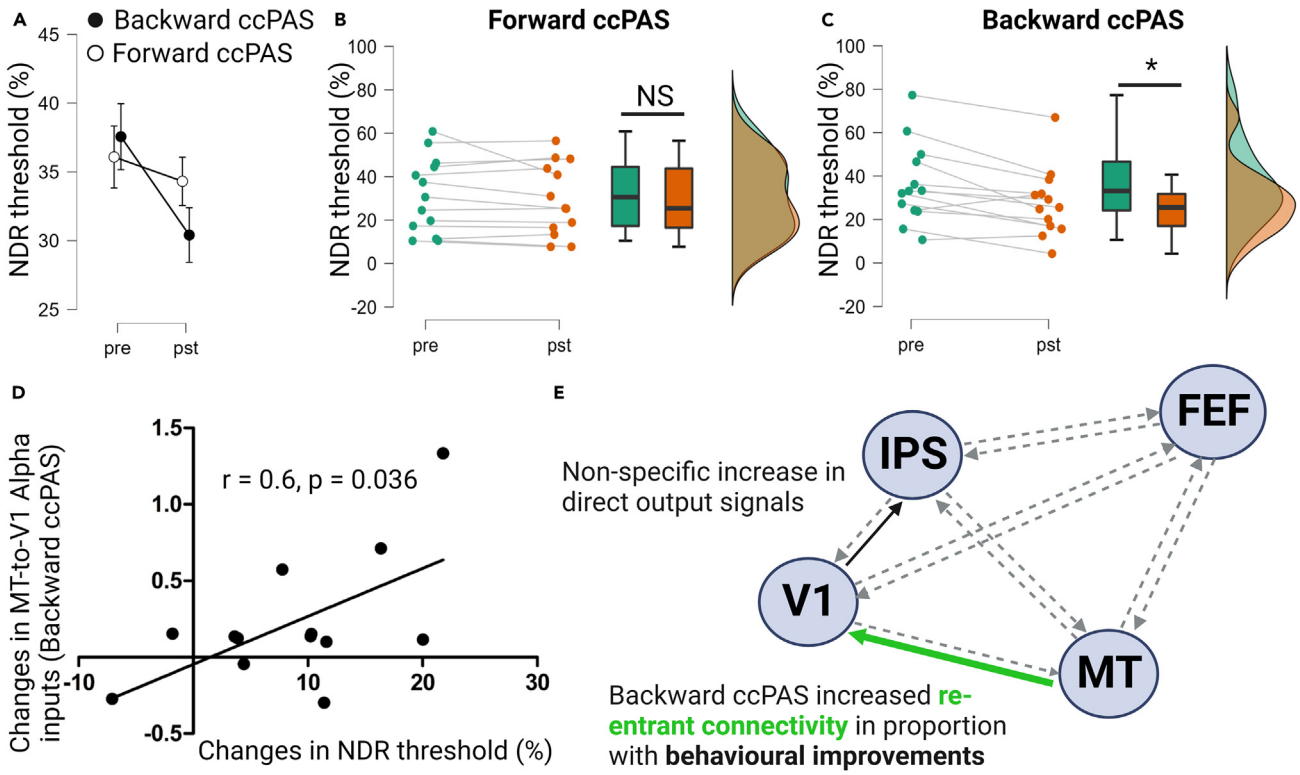

Figure 3. Behavioral results

(A) Group-level changes in NDR thresholds for the two ccPAS conditions.

(B) Individual data and post hoc within group comparison for Forward-ccPAS.

(C) Individual data and post hoc within group comparison for Backward-ccPAS.

(D) Correlational plot between the changes in MT-V1 connectivity strength and the changes in NDR threshold for the Backward-ccPAS illustrating the results of the forward stepward regression model.

(E) Summary of the connectivity and behavioral results.

was only significant in the Backward-ccPAS condition (Backward-ccPAS: $t_{13} = 3.95$, $p = 0.002$, Forward-ccPAS: $t_{14} = 1.43$, $p = 0.17$, paired t tests) (see Figure 3A for group results and Figures 3B and 3C for individual data related to Forward-ccPAS and Backward-ccPAS, respectively). The order effect was not significant ($F_{(1,11)} = 1.21$, $p = 0.29$). Confidence ratings also showed a significant Time x ccPAS type interaction ($F_{(1,14)} = 4390$, $p < 0.001$), reflecting the specific increase in ratings for the Backward-ccPAS group (Backward-ccPAS: $t_{14} = 1.6$, $p = 0.783$; Forward-ccPAS: $t_{15} = 22$, $p < 0.001$, post hoc within group comparisons).

In order to relate the EEG changes described previously (local source activity and Granger causality connectivity strength involving V1 and MT) to these differences in motion direction discrimination after the two interventions, we designed two forward stepwise regression models, the first one with baseline-corrected NDR values belonging to the Forward-ccPAS session and the second with baseline-corrected NDR values belonging to the Backward-ccPAS session as dependent variables. The results showed that the first model (Forward-ccPAS) was not significant, suggesting that none of the connectivity changes could explain changes in NDR in this ccPAS condition. For the second model (Backward-ccPAS), the model was significant and the retained variable was the re-entrant MT-to-V1 pathway (see Table 1 and Figure 3D). These results showed that the significant improvement in behavior found after Backward-ccPAS could be explained by the increase in top-down inputs from MT-to-V1. All the results are summarized in Figure 3E.

DISCUSSION

In the present study, we used a combined TMS-EEG-behavioral paradigm to investigate whether ccPAS between V1 and MT can modulate direction-specific network plasticity and improve motion direction discrimination in young, healthy participants.

Table 1. Multiple regression analyses

Models					Significant predictors		
	Adj. r2	F	Df	p	Variable	Beta	p
Model 1: Forward-ccPAS	0.0	2.05.	1	0.17	–	–	–
Model 2: Backward-ccPAS	0.28	5.68.	1	0.036	Re-entrant MT-V1 (TMS over V1)	0.58 (SD = 0.24)	0.036

Strengthening MT-to-V1 feedback inputs improves global motion processing and awareness

The intervention of interest tested in this study aimed at strengthening synaptic plasticity of MT-to-V1 feedback projections. V1 receives inputs from neighboring area V2 and from a number of higher level cortical areas (including MT, IPS, and FEF), transmitting the outcomes of many cognitive operations such as attention, expectation, or imagination. As a matter of fact, V1 receives considerably more feedback and lateral inputs than forward thalamic afferents.[58] V1 is therefore a processing and integrative center and part of a complex cortical processing cascade. Those modulatory, backward projections from higher visual areas or associative areas are thought to control the gain of thalamocortical inputs to V1 through the activation of glutamatergic receptors, among others.[59–61]

Evidence from macaques[62] and humans[35,63] has shown that back-projections from extrastriate areas to V1 are crucial for motion discrimination. In an earlier study, Romei and colleagues (2016) applied MT-V1 ccPAS (Backward-ccPAS) in healthy subjects and found improved motion coherence discrimination, suggesting plastic changes within this pathway. We provided further evidence for this finding, with a significant enhancement of motion direction discrimination only after Backward-ccPAS and not Forward-ccPAS. Furthermore, Backward-ccPAS significantly improved motion awareness, as evidenced by increased, metacognitive confidence rating, confirming the role of this pathway for motion awareness.[35,63] Of note, confidence ratings have been shown to influence visual discrimination.[64] Therefore, we cannot infer whether ccPAS exerted its effects directly on motion perception, which then impacted confidence ratings or the opposite. Interestingly, previous research has found that the macaque lateral intraparietal area, homolog of the human IPS, plays a crucial role in forming confidence in perceptual decision-making.[42,65,66] Granger causality results did reveal an increase in V1-to-IPS connectivity for both conditions; therefore, strengthening the MT-V1 pathway might also support the neural circuitry of metacognitive judgements of perceptual decision-making, but future studies should be performed to understand how these two brain functions interact with each other.[42]

However, modulating the reciprocal forward projections did not further boost motion direction discrimination or motion awareness. The Forward-ccPAS only showed a small, non-significant improvement that might be related to a well-reported gradual improvement through practice at motion direction discrimination.[67,68] Importantly, the absence of significant improvements justifies the absence of a Sham comparison in this study, and is partly supported by anatomical studies, showing a mixing of early parallel pathways within V1 that result in an apparent lack of compartmentalization in outputs from V1 to extrastriate cortical areas.[69,70] Some researchers have even provided evidence against parallel-processing models of the primate visual system. Furthermore, the fact that the ccPAS protocol was applied at rest might prevent the possibility of a functional routing through specific cortical circuits relevant to motion processing. Finally, neurons projecting directly from V1 to MT are located within layer 4B, closer to the layer 4Cα border, deeper than neurons projecting to other visual areas such as V2 or V3[71] and deeper than MT-projecting neurons to V1, which are mostly located within layer 1.[72] This combination of factors (fibers' density and cortical depth) could explain why the forward inputs are less sensitive to TMS.

Neural correlates of ccPAS

The network-based interventions showed slight local changes in early EEG source activity in response to single-pulse TMS, especially when measured remotely from the stimulation site. We interpret these results as reflecting changes in signal propagation from the stimulated region to the recorded region. In line with the directionality of ccPAS, Forward-ccPAS increased source activity in MT when V1 was stimulated and decreased V1 source activity when MT was stimulated. Similarly, Backward-ccPAS increased source activity in V1 when MT was stimulated, and induced a short window of inhibition of MT source activity in response to single pulse over V1. The Granger causality results provided additional insights on synaptic transmission and information flow within the cortical motion network. While the source activity profiles are computed

from a mixture of signals from all frequency bands, we used spectrally resolved Granger causality[73] to test hypotheses on specific oscillatory channels mediating backward and forward inputs.[37,38] Crucially, the combination of Granger causality measures with single-pulse TMS allowed us to distinguish between direct output signal diffusion from re-entering signal transmission.[74] This distinction was particularly relevant to Backward-ccPAS, where the re-entrant top-down MT-to-V1 connection was significantly increased in the alpha range (8–12 Hz), in proportion with enhanced motion direction discrimination (see Figure 3E for a summary of our findings). In turn, the bottom-up, re-entrant V1-to-MT pathway was decreased in alpha, suggesting that the Backward-ccPAS protocol is highly sensitive to and primarily acts on re-entrant fibers. These findings are in accordance with animal and human electrophysiological studies: alpha oscillations in the visual cortex have been shown to characterize backward processing while gamma waves are thought to mediate forward connectivity.[37,39,75] The changes in interareal coupling we report in the present study might support the hypothesis of a better local and specialized processing after the Backward-ccPAS protocol. Note that the connectivity analysis also revealed a slight but significant decrease in connectivity between MT and V1 after Forward-ccPAS and between V1 and MT in the Backward-ccPAS, suggesting that there might be an associated long-term depression-like effect that occurs concomitantly to the LTP-like effect on the other direction. Interestingly, this was more prominent when the networks were probed with TMS over MT. We can speculate that V1 is more robust to plastic changes while MT shows more flexible patterns of activity as demonstrated earlier.[76]

Conclusion

This study reports the first evidence of pathway-specific plasticity modulation in humans using a causal probe of effective connectivity via the combination of single-pulse TMS and EEG-derived Granger causality. Fundamentally, these results provide evidence that such focality can be achieved non-invasively in humans. Additionally, these results pave the way to new applications in patients. Manipulating top-down signals in the visual system through Backward-ccPAS could be used to quantify the acute capacity of the visual system to reorganize and from this index, extract a predictor for visual recovery potential in pathological states. The "amount" of induced plasticity in hemianopic stroke patients, for instance, could reveal precious information about the functional state of their visual system, and predict whether an individual's brain is able to recruit backward projecting neurons to the spared V1 population to support recovery.[77]

Limitations of the study

A limitation of our study is the small sample size. While we have addressed this limitation by ensuring the features of interest (NDR and GC-based connectivity) have very good test-retest sensitivity levels.[89,90] There is an increasing awareness of the importance of both reliability and reproducibility in brain stimulation studies.[91,92] Therefore, future work should use an independently collected and larger sample to validate our findings. Another limitation is the absence of direct comparison of our bifocal ccPAS stimulation with monofocal V1 or MT stimulation. While we think that this condition was not as relevant for pathway-specific neuromodulation, a few studies have found a modulation of motion discrimination with monofocal stimulation[93,94] but no studies reported any changes in functional connectivity. A last bifocal condition could have been simultaneous V1 and MT stimulation. This control condition has been tested previously and has been shown to have no effect on performances.[51] Finally, it is likely that the effect and magnitude of ccPAS over the MT-to-V1 back projections, potentially mediated by spike timing-dependent plasticity (STDP), might be subject to state-dependent shifts in neocortical excitability.[95–97] These different excitability states could be indexed or indirectly readout using EEG-derived phases of neocortical oscillations, in particular during the alpha cycle.[96] Therefore, to further improve the effects of the Backward-ccPAS intervention, one could implement it in a neocortical-excitability state-dependent framework. Future studies should test whether phase information extracted through online EEG recordings could be used to trigger the paired-pulse TMS over MT and V1, either to control the onset of the paired pulse or the time delay between the conditioning and test pulse (MT and V1 pulse) to ultimately boost its effects.

STAR★METHODS

Detailed methods are provided in the online version of this paper and include the following:

- KEY RESOURCES TABLE
- RESOURCE AVAILABILITY
  - Lead contact
  - Materials availability

ACKNOWLEDGMENTS

We would like to thank the EEG and neuromodulation facilities of the Human Neuroscience Platform of the Fondation Campus Biotech Geneva, for technical advice. This study was supported by the Bertarelli Foundation (Catalyst BC77O7 to F.C.H. & E.R.), by the Swiss National Science Foundation (PRIMA PR00P3_179867 to E.R.), and by the Defitech Foundation (to F.C.H.).

AUTHOR CONTRIBUTIONS

M.B., E.R., and F.C.H. conceived the concept of the study, designed the research, M.B. and E.R. wrote the manuscript. M.B. and E.R. conducted the experiments. M.B. and E.R. analyzed the data. F.C.H. and K.H. revised the manuscript. E.R. and F.C.H. acquired funding support.

DECLARATION OF INTERESTS

The authors declare no competing interests.

INCLUSION AND DIVERSITY

We support inclusive, diverse, and equitable conduct of research.

Received: June 23, 2022
Revised: February 14, 2023
Accepted: June 2, 2023
Published: June 7, 2023

REFERENCES

1. Felleman, D.J., and Van Essen, D.C. (1991). Distributed hierarchical processing in the primate cerebral cortex. Cereb. Cortex *1*, 1–47. https://doi.org/10.1093/cercor/1.1.1.

2. Catani, M., Jones, D.K., Donato, R., and Ffytche, D.H. (2003). Occipito-temporal connections in the human brain. Brain *126*, 2093–2107. https://doi.org/10.1093/brain/awg203.

3. Antal, A., Kincses, T.Z., Nitsche, M.A., Bartfai, O., and Paulus, W. (2004). Excitability changes induced in the human primary visual cortex by transcranial direct current stimulation: direct electrophysiological evidence. Invest. Ophthalmol. Vis. Sci. *45*, 702–707.

4. Bressler, S.L., Tang, W., Sylvester, C.M., Shulman, G.L., and Corbetta, M. (2008). Top-down control of human visual cortex by frontal and parietal cortex in anticipatory visual spatial attention. J. Neurosci. *28*, 10056–10061. https://doi.org/10.1523/JNEUROSCI.1776-08.2008.

5. Reynolds, J.H., and Desimone, R. (2003). Interacting roles of attention and visual salience in V4. Neuron *37*, 853–863. https://doi.org/10.1016/s0896-6273(03)00097-7.

6. Mikami, A., Newsome, W.T., and Wurtz, R.H. (1986). Motion selectivity in macaque visual cortex. I. Mechanisms of direction and speed selectivity in extrastriate area MT. J. Neurophysiol. *55*, 1308–1327. https://doi.org/10.1152/jn.1986.55.6.1308.

7. Hubel, D.H., and Wiesel, T.N. (1968). Receptive fields and functional architecture of monkey striate cortex. J. Physiol. *195*, 215–243. https://doi.org/10.1113/jphysiol.1968.sp008455.

8. Gizzi, M.S., Katz, E., Schumer, R.A., and Movshon, J.A. (1990). Selectivity for orientation and direction of motion of single neurons in cat striate and extrastriate visual cortex. J. Neurophysiol. *63*, 1529–1543. https://doi.org/10.1152/jn.1990.63.6.1529.

9. Maunsell, J.H., and Van Essen, D.C. (1983). Functional properties of neurons in middle temporal visual area of the macaque monkey. I. Selectivity for stimulus direction, speed, and orientation. J. Neurophysiol. *49*, 1127–1147. https://doi.org/10.1152/jn.1983.49.5.1127.

10. Movshon, J.A., and Newsome, W.T. (1996). Visual response properties of striate cortical neurons projecting to area MT in macaque monkeys. J. Neurosci. *16*, 7733–7741. https://doi.org/10.1523/JNEUROSCI.16-23-07733.1996.

11. Maunsell, H.R., and Van, C. (1983). The connections of the middle temporal visual area (MT) and their relationship to a cortical hierarchy in the macaque monkey. J. Neurosci. *3*, 24.

12. Albright, T.D., Desimone, R., and Gross, C.G. (1984). Columnar organization of directionally selective cells in visual area MT of the macaque. J. Neurophysiol. *51*, 16–31. https://doi.org/10.1152/jn.1984.51.1.16.

13. Britten, K.H., Newsome, W.T., Shadlen, M.N., Celebrini, S., and Movshon, J.A. (1996). A relationship between behavioral choice and the visual responses of neurons in macaque MT. Vis. Neurosci. *13*, 87–100. https://doi.org/10.1017/S095252380000715X.

14. Gamberini, M., Bakola, S., Passarelli, L., Burman, K.J., Rosa, M.G.P., Fattori, P., and Galletti, C. (2016). Thalamic projections to visual and visuomotor areas (V6 and V6A) in the Rostral Bank of the parieto-occipital sulcus of the Macaque. Brain Struct. Funct. *221*, 1573–1589. https://doi.org/10.1007/s00429-015-0990-2.

15. Pitzalis, S., Sereno, M.I., Committeri, G., Fattori, P., Galati, G., Patria, F., and Galletti, C. (2010). Human V6: the medial motion area. Cereb. Cortex *20*, 411–424. https://doi.org/10.1093/cercor/bhp112.

16. Felleman, D.J., and Van Essen, D.C. (1987). Receptive field properties of neurons in area V3 of macaque monkey extrastriate cortex. J. Neurophysiol. *57*, 889–920. https://doi.org/10.1152/jn.1987.57.4.889.

17. Lagae, L., Raiguel, S., and Orban, G.A. (1993). Speed and direction selectivity of macaque middle temporal neurons. J. Neurophysiol. *69*, 19–39. https://doi.org/10.1152/jn.1993.69.1.19.

18. Perrone, J.A., and Thiele, A. (2001). Speed skills: measuring the visual speed analyzing properties of primate MT neurons. Nat. Neurosci. *4*, 526–532. https://doi.org/10.1038/87480.

19. Rodman, H.R., and Albright, T.D. (1987). Coding of visual stimulus velocity in area MT of the macaque. Vision Res. *27*, 2035–2048. https://doi.org/10.1016/0042-6989(87)90118-0.

20. Das, A., Tadin, D., and Huxlin, K.R. (2014). Beyond blindsight: properties of visual relearning in cortically blind fields. J. Neurosci. *34*, 11652–11664. https://doi.org/10.1523/JNEUROSCI.1076-14.2014.

21. Huxlin, K.R., Martin, T., Kelly, K., Riley, M., Friedman, D.I., Burgin, W.S., and Hayhoe, M. (2009). Perceptual relearning of complex visual motion after V1 damage in humans. J. Neurosci. *29*, 3981–3991. https://doi.org/10.1523/JNEUROSCI.4882-08.2009.

22. Pasternak, T., and Merigan, W.H. (1994). Motion perception following lesions of the superior temporal sulcus in the monkey. Cereb. Cortex *4*, 247–259. https://doi.org/10.1093/cercor/4.3.247.

23. Marcar, V.L., and Cowey, A. (1992). The effect of removing superior temporal cortical motion areas in the macaque monkey: II. Motion discrimination using random dot displays. Eur. J. Neurosci. *4*, 1228–1238. https://doi.org/10.1111/j.1460-9568.1992.tb00148.x.

24. Newsome, W.T., and Paré, E.B. (1988). A selective impairment of motion perception following lesions of the middle temporal visual area (MT). J. Neurosci. *8*, 2201–2211. https://doi.org/10.1523/JNEUROSCI.08-06-02201.1988.

25. Rudolph, K., and Pasternak, T. (1999). Transient and permanent deficits in motion perception after lesions of cortical areas MT and MST in the macaque monkey. Cereb. Cortex *9*, 90–100. https://doi.org/10.1093/cercor/9.1.90.

26. Cowey, A., and Walsh, V. (2001). Chapter 26 Tickling the brain: studying visual sensation, perception and cognition by transcranial magnetic stimulation. In Progress in Brain Research (Elsevier), pp. 411–425. https://doi.org/10.1016/S0079-6123(01)34027-X.

27. Ellison, A., Battelli, L., Cowey, A., and Walsh, V. (2003). The effect of expectation on facilitation of colour/form conjunction tasks by TMS over area V5. Neuropsychologia *41*, 1794–1801. https://doi.org/10.1016/S0028-3932(03)00180-5.

28. Krug, K., Cicmil, N., Parker, A.J., and Cumming, B.G. (2013). A causal role for V5/MT neurons coding motion-disparity conjunctions in resolving perceptual ambiguity. Curr. Biol. *23*, 1454–1459. https://doi.org/10.1016/j.cub.2013.06.023.

29. Ruzzoli, M., Marzi, C.A., and Miniussi, C. (2010). The neural mechanisms of the effects of transcranial magnetic stimulation on perception. J. Neurophysiol. *103*, 2982–2989. https://doi.org/10.1152/jn.01096.2009.

30. Tononi, G., Sporns, O., and Edelman, G.M. (1992). Reentry and the problem of integrating multiple cortical areas: simulation of dynamic integration in the visual system. Cereb. Cortex *2*, 310–335. https://doi.org/10.1093/cercor/2.4.310.

31. Pan, H., Zhang, S., Pan, D., Ye, Z., Yu, H., Ding, J., Wang, Q., Sun, Q., and Hua, T. (2020). Characterization of feedback neurons in the high-level visual cortical areas that project directly to the primary visual cortex in the cat. Front. Neuroanat. *14*, 616465.

32. Wibral, M., Bledowski, C., Kohler, A., Singer, W., and Muckli, L. (2009). The timing of feedback to early visual cortex in the perception of long-range apparent motion. Cereb. Cortex *19*, 1567–1582. https://doi.org/10.1093/cercor/bhn192.

34. Laycock, R., Crewther, D.P., Fitzgerald, P.B., and Crewther, S.G. (2007). Evidence for fast signals and later processing in human V1/V2 and V5/MT+: a TMS study of motion perception. J. Neurophysiol. *98*, 1253–1262. https://doi.org/10.1152/jn.00416.2007.

35. Pascual-Leone, A., and Walsh, V. (2001). Fast backprojections from the motion to the primary visual area necessary for visual awareness. Science *292*, 510–512. https://doi.org/10.1126/science.1057099.

36. Silvanto, J. (2015). Why is "blindsight" blind? A new perspective on primary visual cortex, recurrent activity and visual awareness. Conscious. Cogn. *32*, 15–32. https://doi.org/10.1016/j.concog.2014.08.001.

37. van Kerkoerle, T., Self, M.W., Dagnino, B., Gariel-Mathis, M.-A., Poort, J., van der Togt, C., and Roelfsema, P.R. (2014). Alpha and gamma oscillations characterize feedback and feedforward processing in monkey visual cortex. Proc. Natl. Acad. Sci. USA *111*, 14332–14341. https://doi.org/10.1073/pnas.1402773111.

38. Bastos, A.M., Vezoli, J., Bosman, C.A., Schoffelen, J.-M., Oostenveld, R., Dowdall, J.R., De Weerd, P., Kennedy, H., and Fries, P. (2015). Visual areas exert feedforward and feedback influences through distinct frequency channels. Neuron *85*, 390–401. https://doi.org/10.1016/j.neuron.2014.12.018.

39. Michalareas, G., Vezoli, J., van Pelt, S., Schoffelen, J.-M., Kennedy, H., and Fries, P. (2016). Alpha-beta and gamma rhythms subserve feedback and feedforward influences among human visual cortical areas. Neuron *89*, 384–397. https://doi.org/10.1016/j.neuron.2015.12.018.

40. Casarotto, S., Fecchio, M., Rosanova, M., Varone, G., D'Ambrosio, S., Sarasso, S., Pigorini, A., Russo, S., Comanducci, A., Ilmoniemi, R.J., and Massimini, M. (2022). The rt-TEP tool: real-time visualization of TMS-evoked potentials to maximize cortical activation and minimize artifacts. J. Neurosci. Methods *370*, 109486. https://doi.org/10.1016/j.jneumeth.2022.109486.

41. Chiappini, E., Silvanto, J., Hibbard, P.B., Avenanti, A., and Romei, V. (2018). Strengthening functionally specific neural pathways with transcranial brain stimulation. Curr. Biol. *28*, R735–R736. https://doi.org/10.1016/j.cub.2018.05.083.

42. Di Luzio, P., Tarasi, L., Silvanto, J., Avenanti, A., and Romei, V. (2022). Human perceptual and metacognitive decision-making rely on distinct brain networks. PLoS Biol. *20*, e3001750. https://doi.org/10.1371/journal.pbio.3001750.

43. Fiori, F., Chiappini, E., and Avenanti, A. (2018). Enhanced action performance following TMS manipulation of associative plasticity in ventral premotor-motor pathway. Neuroimage *183*, 847–858. https://doi.org/10.1016/j.neuroimage.2018.09.002.

44. Rizzo, V., Siebner, H.S., Morgante, F., Mastroeni, C., Girlanda, P., and Quartarone, A. (2009). Paired associative stimulation of left and right human motor cortex shapes interhemispheric motor inhibition based on a Hebbian mechanism. Cereb. Cortex *19*, 907–915. https://doi.org/10.1093/cercor/bhn144.

45. Turrini, S., Fiori, F., Chiappini, E., Santarnecchi, E., Romei, V., and Avenanti, A. (2022). Gradual enhancement of corticomotor excitability during cortico-cortical paired associative stimulation. Sci. Rep. *12*, 14670. https://doi.org/10.1038/s41598-022-18774-9.

46. Magee, J.C., and Johnston, D. (1997). A synaptically controlled, associative signal for

Hebbian plasticity in Hippocampal neurons. Science *275*, 209–213. https://doi.org/10.1126/science.275.5297.209.

47. Stefan, K., Kunesch, E., Cohen, L.G., Benecke, R., and Classen, J. (2000). Induction of plasticity in the human motor cortex by paired associative stimulation. Brain *123 Pt 3*, 572–584. https://doi.org/10.1093/brain/123.3.572.

48. Caporale, N., and Dan, Y. (2008). Spike timing–dependent plasticity: a Hebbian learning rule. Annu. Rev. Neurosci. *31*, 25–46. https://doi.org/10.1146/annurev.neuro.31.060407.125639.

49. Koch, G. (2020). Cortico-cortical connectivity: the road from basic neurophysiological interactions to therapeutic applications. Exp. Brain Res. *238*, 1677–1684. https://doi.org/10.1007/s00221-020-05844-5.

50. Spampinato, D.A., Block, H.J., and Celnik, P.A. (2017). Cerebellar–M1 connectivity changes associated with motor learning are somatotopic specific. J. Neurosci. *37*, 2377–2386. https://doi.org/10.1523/JNEUROSCI.2511-16.2017.

51. Romei, V., Chiappini, E., Hibbard, P.B., and Avenanti, A. (2016). Empowering reentrant projections from V5 to V1 boosts sensitivity to motion. Curr. Biol. *26*, 2155–2160. https://doi.org/10.1016/j.cub.2016.06.009.

52. Keil, A., Sabatinelli, D., Ding, M., Lang, P.J., Ihssen, N., and Heim, S. (2009). Re-entrant projections modulate visual cortex in affective perception: evidence from Granger causality analysis. Hum. Brain Mapp. *30*, 532–540. https://doi.org/10.1002/hbm.20521.

53. Friston, K.J., Stephan, K.E., Montague, R., and Dolan, R.J. (2014). Computational psychiatry: the brain as a phantastic organ. Lancet Psychiatr. *1*, 148–158. https://doi.org/10.1016/S2215-0366(14)70275-5.

54. Martin, T., Huxlin, K.R., and Kavcic, V. (2010). Motion-onset visual evoked potentials predict performance during a global direction discrimination task. Neuropsychologia *48*, 3563–3572. https://doi.org/10.1016/j.neuropsychologia.2010.08.005.

55. Raffin, E., Witon, A., Salamanca-Giron, R.F., Huxlin, K.R., and Hummel, F.C. (2022). Functional segregation within the dorsal frontoparietal network: a multimodal dynamic causal modeling study. Cereb. Cortex *32*, 3187–3205. 1991, bhab409. https://doi.org/10.1093/cercor/bhab409.

56. Saionz, E.L., Tadin, D., Melnick, M.D., and Huxlin, K.R. (2020). Functional preservation and enhanced capacity for visual restoration in subacute occipital stroke. Brain *143*, 1857–1872. https://doi.org/10.1093/brain/awaa128.

57. Salamanca-Giron, R.F., Raffin, E., Zandvliet, S.B., Seeber, M., Michel, C.M., Sauseng, P., Huxlin, K.R., and Hummel, F.C. (2021). Enhancing visual motion discrimination by desynchronizing bifocal oscillatory activity. Neuroimage *240*, 118299. https://doi.org/10.1016/j.neuroimage.2021.118299.

58. Budd, J.M. (1998). Extrastriate feedback to primary visual cortex in primates: a quantitative analysis of connectivity. Proc. Biol. Sci. *265*, 1037–1044.

59. Ekstrom, L.B., Roelfsema, P.R., Arsenault, J.T., Bonmassar, G., and Vanduffel, W. (2008). Bottom-up dependent gating of frontal signals in early visual cortex. Science *321*, 414–417. https://doi.org/10.1126/science.1153276.

60. Hupé, J.M., James, A.C., Girard, P., Lomber, S.G., Payne, B.R., and Bullier, J. (2001). Feedback connections act on the early part of the responses in monkey visual cortex. J. Neurophysiol. *85*, 134–145. https://doi.org/10.1152/jn.2001.85.1.134.

61. Muckli, L., and Petro, L.S. (2013). Network interactions: non-geniculate input to V1. Curr. Opin. Neurobiol. *23*, 195–201. https://doi.org/10.1016/j.conb.2013.01.020.

62. Lamme, V.A., Supèr, H., and Spekreijse, H. (1998). Feedforward, horizontal, and feedback processing in the visual cortex. Curr. Opin. Neurobiol. *8*, 529–535. https://doi.org/10.1016/S0959-4388(98)80042-1.

63. Silvanto, J., Cowey, A., Lavie, N., and Walsh, V. (2005). Striate cortex (V1) activity gates awareness of motion. Nat. Neurosci. *8*, 143–144. https://doi.org/10.1038/nn1379.

64. Bonder, T., and Gopher, D. (2019). The effect of confidence rating on a primary visual task. Front. Psychol. *10*, 2674. https://doi.org/10.3389/fpsyg.2019.02674.

65. Huk, A.C., Katz, L.N., and Yates, J.L. (2017). The role of the lateral intraparietal area in (the study of) decision making. Annu. Rev. Neurosci. *40*, 349–372. https://doi.org/10.1146/annurev-neuro-072116-031508.

66. Pasternak, T., and Tadin, D. (2020). Linking neuronal direction selectivity to perceptual decisions about visual motion. Annu. Rev. Vis. Sci. *6*, 335–362. https://doi.org/10.1146/annurev-vision-121219-081816.

67. Gibson, E.J. (1963). Perceptual learning. Annu. Rev. Psychol. *14*, 29–56. https://doi.org/10.1146/annurev.ps.14.020163.000333.

68. Sagi, D. (2011). Perceptual learning in vision research. Vision Res. *51*, 1552–1566. https://doi.org/10.1016/j.visres.2010.10.019.

69. Sincich, L.C., Park, K.F., Wohlgemuth, M.J., and Horton, J.C. (2004). Bypassing V1: a direct geniculate input to area MT. Nat. Neurosci. *7*, 1123–1128. https://doi.org/10.1038/nn1318.

70. Xiao, Y., and Felleman, D.J. (2004). Projections from primary visual cortex to cytochrome oxidase thin stripes and interstripes of macaque visual area 2. Proc. Natl. Acad. Sci. USA *101*, 7147–7151. https://doi.org/10.1073/pnas.0402052101.

71. Nassi, J.J., and Callaway, E.M. (2007). Specialized circuits from primary visual cortex to V2 and area MT. Neuron *55*, 799–808. https://doi.org/10.1016/j.neuron.2007.07.037.

72. Blasdel, G.G., and Lund, J.S. (1983). Termination of afferent axons in macaque striate cortex. J. Neurosci. *3*, 1389–1413.

73. Chicharro, D. (2011). On the spectral formulation of Granger causality. Biol. Cybern. *105*, 331–347. https://doi.org/10.1007/s00422-011-0469-z.

74. Winkler, I., Haufe, S., Porbadnigk, A.K., Müller, K.R., and Dähne, S. (2015). Identifying Granger causal relationships between neural power dynamics and variables of interest. Neuroimage *111*, 489–504. https://doi.org/10.1016/j.neuroimage.2014.12.059.

75. Richter, C.G., Coppola, R., and Bressler, S.L. (2018). Top-down beta oscillatory signaling conveys behavioral context in early visual cortex. Sci. Rep. *8*, 6991. https://doi.org/10.1038/s41598-018-25267-1.

76. Raffin, E., Witon, A., Salamanca-Giron, R.F., Huxlin, K.R., and Hummel, F.C. (2022). Functional segregation within the dorsal frontoparietal network: a multimodal dynamic causal modeling study. Cereb. Cortex *32*, 3187–3205. https://doi.org/10.1093/cercor/bhab409.

77. Barbot, A., Das, A., Melnick, M.D., Cavanaugh, M.R., Merriam, E.P., Heeger, D.J., and Huxlin, K.R. (2021). Spared perilesional V1 activity underlies training-induced recovery of luminance detection sensitivity in cortically-blind patients. Nat. Commun. *12*, 6102. https://doi.org/10.1038/s41467-021-26345-1.

78. Oostenveld, R., Fries, P., Maris, E., and Schoffelen, J.-M. (2011). FieldTrip: open source software for advanced analysis of MEG, EEG, and invasive electrophysiological data. Comput. Intell. Neurosci. *2011*, 156869. https://doi.org/10.1155/2011/156869.

79. Tadel, F., Baillet, S., Mosher, J.C., Pantazis, D., and Leahy, R.M. (2011). Brainstorm: a user-friendly application for MEG/EEG analysis. Comput. Intell. Neurosci. *2011*, 879716–879813. https://doi.org/10.1155/2011/879716.

80. Rossi, S., Antal, A., Bestmann, S., Bikson, M., Brewer, C., Brockmöller, J., Carpenter, L.L., Cincotta, M., Chen, R., Daskalakis, J.D., et al. (2021). Safety and recommendations for TMS use in healthy subjects and patient populations, with updates on training, ethical and regulatory issues: expert Guidelines. Clin. Neurophysiol. *132*, 269–306. https://doi.org/10.1016/j.clinph.2020.10.003.

81. Gerwig, M., Kastrup, O., Meyer, B.-U., and Niehaus, L. (2003). Evaluation of cortical excitability by motor and phosphene thresholds in transcranial magnetic stimulation. J. Neurol. Sci. *215*, 75–78. https://doi.org/10.1016/S0022-510X(03)00228-4.

83. Jackson, A., Mavoori, J., and Fetz, E.E. (2006). Long-term motor cortex plasticity induced by an electronic neural implant *444*, 56–60.

84. Rogasch, N.C., Sullivan, C., Thomson, R.H., Rose, N.S., Bailey, N.W., Fitzgerald, P.B.,

Farzan, F., and Hernandez-Pavon, J.C. (2017). Analysing concurrent transcranial magnetic stimulation and electroencephalographic data: a review and introduction to the open-source TESA software. Neuroimage *147*, 934–951. https://doi.org/10.1016/j.neuroimage.2016.10.031.

85. Tadel, F., Baillet, S., Mosher, J.C., Pantazis, D., and Leahy, R.M. (2011). Brainstorm: a user-friendly application for MEG/EEG analysis. Comput. Intell. Neurosci. *2011*, 879716. https://doi.org/10.1155/2011/879716.

86. Gramfort, A., Papadopoulo, T., Olivi, E., and Clerc, M. (2010). OpenMEEG: opensource software for quasistatic bioelectromagnetics. Biomed. Eng. Online *9*, 45. https://doi.org/10.1186/1475-925X-9-45.

87. West, T.O. (2020). Measuring directed functional connectivity using non-parametric directionality analysis: validation and comparison with non-parametric granger causality *19*.

88. Lage-Castellanos, A., Martínez-Montes, E., Hernández-Cabrera, J.A., and Galán, L. (2009). False discovery rate and permutation test: an evaluation in ERP data analysis *12*.

89. Franciotti, R., and Falasca, N. (2018). The reliability of conditional granger causality analysis in the time domain. PeerJ. Preprint at bioRxiv. https://doi.org/10.7287/peerj.preprints.26703v1.

90. Krit, M., Gaudoin, O., and Remy, E. (2021). Goodness-of-fit tests for the Weibull and extreme value distributions: a review and comparative study. Commun. Stat. - Simul. Comput. *50*, 1888–1911. https://doi.org/10.1080/03610918.2019.1594292.

91. Héroux, M.E., Loo, C.K., Taylor, J.L., and Gandevia, S.C. (2017). Questionable science and reproducibility in electrical brain stimulation research. PLoS One *12*, e0175635. https://doi.org/10.1371/journal.pone.0175635.

92. Bikson, M., Brunoni, A.R., Charvet, L.E., Clark, V.P., Cohen, L.G., Deng, Z.-D., Dmochowski, J., Edwards, D.J., Frohlich, F., Kappenman, E.S., et al. (2018). Rigor and reproducibility in research with transcranial electrical stimulation: an NIMH-sponsored workshop. Brain Stimul. *11*, 465–480. https://doi.org/10.1016/j.brs.2017.12.008.

93. Thompson, B., Deblieck, C., Wu, A., Iacoboni, M., and Liu, Z. (2016). Psychophysical and rTMS evidence for the presence of motion opponency in human V5. Brain Stimul. *9*, 876–881. https://doi.org/10.1016/j.brs.2016.05.012.

94. Waterston, M.L., and Pack, C.C. (2010). Improved discrimination of visual stimuli following repetitive transcranial magnetic stimulation. PLoS One *5*, e10354. https://doi.org/10.1371/journal.pone.0010354.

95. Chao, C.-C., Karabanov, A.N., Paine, R., Carolina de Campos, A., Kukke, S.N., Wu, T., Wang, H., and Hallett, M. (2015). Induction of motor associative plasticity in the posterior parietal cortex-primary motor network. Cereb. Cortex *25*, 365–373. https://doi.org/10.1093/cercor/bht230.

96. Fehér, K.D., Nakataki, M., and Morishima, Y. (2017). Phase-dependent modulation of signal transmission in cortical networks through tACS-induced neural oscillations. Front. Hum. Neurosci. *11*, 471. https://doi.org/10.3389/fnhum.2017.00471.

97. Koch, G., Ponzo, V., Di Lorenzo, F., Caltagirone, C., and Veniero, D. (2013). Hebbian and anti-Hebbian spike-timing-dependent plasticity of human cortico-cortical connections. J. Neurosci. *33*, 9725–9733. https://doi.org/10.1523/JNEUROSCI.4988-12.2013.

STAR★METHODS

KEY RESOURCES TABLE

REAGENT or RESOURCE	SOURCE	IDENTIFIER
Software and algorithms		
Custom code	This study	Available upon request
FieldTrip	Oostenveld et al.[78]	Git commit 4c12371
MATLAB	Mathworks	R2019a
Brainstorm	Tadel et al.[80]	https://neuroimage.usc.edu/brainstorm

RESOURCE AVAILABILITY

Lead contact

Further information and requests for resources and reagents should be directed to and will be fulfilled by the lead contact, Estelle Raffin (estelle.raffin@epfl.ch).

Materials availability

This study did not generate new unique reagents.

Data and code availability

- Extracted behavioural and Granger Causality data are made available in the Zenodo Database: https://doi.org/10.5281/zenodo.7969185.
- This paper does not report original code.
- Any additional information required to reanalyse the data reported in this paper is available from the lead contact upon request.

EXPERIMENTAL MODEL AND SUBJECT DETAILS

16 healthy subjects (9 F, 7M, mean ± SD age: 27 ± 4 years) participated in the study. All participants provided informed, written consent prior the experiment and none of them met the MRI or TMS exclusion criteria.[80] This study was approved by the local Swiss Ethics Committee (2017-01761) and performed in accordance with the Declaration of Helsinki.

METHOD DETAILS

General procedures

This double-blinded and cross-over study involved two sessions of 3 hours each, only differing by the type of ccPAS intervention applied to the participants. The two sessions were performed at least one month apart and the order was randomized and counter-balanced between participants. Each session comprised a familiarization phase including 3 blocks of 20 trials each, to ensure that the subjects understood the visual discrimination task and reached stable performance. After EEG cap preparation, TMS sites and intensities were defined (see below for more details). Task performances and EEG responses to single pulses over V1 and MT were measured at baseline, followed by one of the two ccPAS interventions. Ten minutes after the end of the ccPAS, task performances and single pulse TMS-EEG over V1 and MT were measured again. During the whole experiment, the participants sat on a chair, with the head leaning on the chinrest, in front of a computer screen, centred 47 cm far from the eyes. Every subject was asked to fill in a short questionnaire related to eventual issues and inconveniences caused by the single pulse TMS or ccPAS intervention at the end of both sessions.

Please see below figure

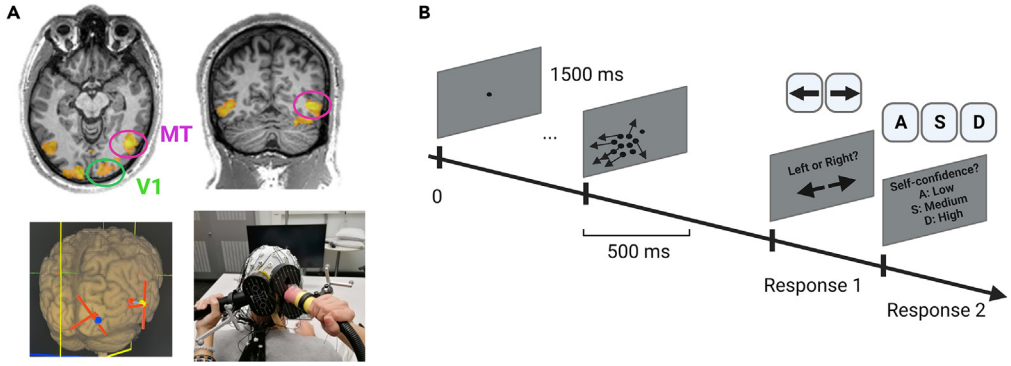

Brain stimulation and behavioral measurements

(A) Example of an individual functional localizer, online neuronavigation, and coil positioning.

(B) The motion direction discrimination and integration task used before and after the ccPAS interventions.

Single pulse TMS

For single-pulse TMS over V1 and MT, biphasic TMS pulses inducing an antero-posterior followed by postero-anterior current in the brain (AP-PA) were sent through a MC-B65-HO butterfly coil (MagVenture A/S, Denmark) plugged in a MagPro XP TMS stimulator (MagVenture A/S, Denmark). Pulses duration was 200 μs for MagPro 100 and 300 μs for the MagPro XP, delivered through continuous neuronavigation monitoring using the Localite neuronavigation software (Localite GmbH, Germany).

To determine stimulation intensities, we evaluated the phosphene threshold[81] on both V1 and MT. If the participants reported phosphenes (9/16 for V1 and 5/16 for MT), we set the stimulation intensity at 90% of the phosphene's threshold. If no phosphenes could be evoked, we used 65 % of the maximal stimulator's output (MSO) in all participants to maximize signal-to-noise ratio and comfort during the exam. Because of discomfort related to the fact that MT is located close to the ear, we decreased the intensity to 60% MSO. The mean stimulation intensity for V1 was 66±6 % MSO and for MT 61±4 % MSO. On each area, 90 TMS pulses were performed with an inter-pulse interval of 4±1s. Stimulation intensities were re-evaluated at the beginning of the second session and adjusted if needed.

To precisely target individual V1 and MT areas, we used a standard fMRI MT localizer task performed prior the TMS-EEG session (see above figure). During the functional localizer, the screen displayed radially moving dots alternating with stationary dots (see e.g. Sack et al., 2007). A block design alternated six 15 s blocks of radial motion with six blocks featuring stationary white dots in a circular region on a black background. This region subtended 25° visual angle, with 0.5 dots per square degree. Each dot was 0.36° diameter. In the motion condition the dots repeatedly moved radially inward for 2.5 s and outward for 2.5 s, with 100% coherence, at 20°/s measured at 15° from the center. Participants were passively looking at the screen and were asked to focus on a fixation point located in the middle of the screen. The resulting activation map and the individual T1 image were entered into the neuro-navigation software to define the coil positions (see above figure). The mean coil positions for V1 were -16±9, -86±8, -5±22 and for MT were 66±9, -55±9, -7±17 (coordinates x, y z, MNI space). The coil was held tangentially to the scalp with the handle pointing upwards and laterally at 45° angle to the sagittal plane.

ccPAS interventions

ccPAS was delivered via two independent TMS stimulators externally triggered with Signal (Digitimer, Cambridge Electronic Design, Cambridge, UK). MT was stimulated using the same stimulator/coil combination than for single pulse TMS-EEG recordings, i.e., with a MagVenture MagPro XP stimulator (MagVenture A/S, Denmark) connected to a MC-B65-HO coil. The right MT area was stimulated with a MagVenture MagPro X100 stimulator connected to a smaller coil to allow precise anatomical targeting, i.e., the MC-B35 coil. The same coil positions used for single TMS were applied for the ccPAS procedure, with both coils being neuronavigated (see above figure). The same intensities were used for MT. For V1,

since we used a different coil, we recalibrated the stimulation intensity to match the single pulse TMS condition. 90 pairs of biphasic stimuli were continuously delivered at a rate of 0.1 Hz for 15 min. The coil handle for MT was held tangentially to the scalp and pointed downwards at an angle of 120° ±5 clockwise.

Because our goal was to explore direction-specificity effects of ccPAS in the motion processing network, we compared two types of ccPAS, differing by the order of the two pulses. In the backward MT-V1 ccPAS condition *(Backward-ccPAS)*, the first TMS pulse was applied to MT followed by a pulse to V1. In the forward V1-MT ccPAS condition *(Forward-ccPAS)*, the TMS pulses order was reversed; the first pulse was administered to V1 and the second to MT (see above figure). The inter-stimulus interval (ISI) was set at 20ms for both ccPAS conditions, because it corresponds to the time delays of MT-V1 back projections.[35,63] This timing is critical to create sequential presynaptic and postsynaptic activity in the network, and to generate the occurrence of STDP.[48,83]

Behavioural task

We used a well-established 2-alternative, forced-choice, left-right, global direction discrimination and integration task (150 trials in total), as previously described.[21,54–57] Subjects were asked to discriminate the left–right direction of motion of random-dot stimuli. They performed 150 trials, with each trial initiated by fixation of a small spot of light within an electronic window 2 × 2° in size. Steady fixation of this target for 1000 ms resulted in a tone signaling the onset of stimulus presentation during which subjects were required to maintain fixation. A break in fixation during stimulus presentation produced a loud, 1 s tone and the termination of the trial. After 500 ms, the stimulus and fixation spot disappeared, and the subjects were required to indicate whether they perceived the global direction of motion of the stimulus to be toward the right or the left by pressing the right or left arrow key on a computer keyboard placed in front of them. Correct and incorrect responses were signaled by different computer-generated tones, so that the subjects instantly knew whether they performed correctly or not. The sequence of presentation of rightward and leftward drifting stimuli was randomized. The degree of difficulty or direction range was increased with task performance by increasing the range of dot directions within the stimulus using a 3:1 staircase design. For every 3 consecutive correct trials, direction range increased by 40°, while for every incorrect response, it decreased by 40°.

Stimuli consisted of a group of black dots moving globally left- or rightwards, with a density of 2.6 dots/deg^2 in a 5°-diameter circular aperture centred at cartesian coordinates [-5°, 5°] (i.e., the bottom left quadrant of the visual field, relative to central fixation (see above figure). The dots moved at a speed of 10°/s for a lifetime of 250 ms (half the stimulus duration). Self-confidence was rated (low/medium/high) after each trial. After each trial, auditory feedback indicated whether the response was correct or incorrect.

The task was implemented in Matlab 2019b (Version 1.8, The MathWorks Inc., USA) coupled with an EyeLink 1000 Plus Eye Tracking System (SR Research Ltd., Canada) sampling at a frequency of 1000 Hz to control gaze and pupil movements in real time. The task was projected onto a mid-grey background LCD projector (1024 x 768 Hz, 144 Hz). Participants used the left-right arrows of the keyboard to respond with their right hand; they pressed "a", "s" or "d" to indicate low/medium/high confidence respectively, on a trial-by-trial basis.

EEG recordings

EEG was recorded using a 64-channels, TMS-compatible system (BrainAmp DC amplifiers and BrainCap EEG cap, Brain Products GmbH, Germany) with the ground electrode at Fpz, the reference electrode at Cz, and the Iz electrode added to the international standard 10-20 layout. Electrode impedances were adjusted and kept under 5 kOhms using conduction gel. The impedance levels were checked throughout the experiment and corrected if needed during breaks between the recordings. The signal was recorded using DC mode, filtered with an 500 Hz anti-aliasing low-pass filter, and digitalized at 5 kHz sampling frequency. Channel coordinates were individually assessed using the neuro-navigation software at the end of the experiment. We used active noise cancellation intra-auricular earphones (Bose QC 20, USA) to mask the TMS click susceptible to evoked auditory responses on the ongoing EEG activity. The sound level was adjusted for each subject, so that the TMS click delivered became barely audible without any discomfort for the participant. A thin layer of soft plastic was placed on the coil surface to dampen both sensory and auditory feedback to the subjects.

TMS-EEG pre-processing

EEG analysis was performed on the EEG recordings of the 90 single pulses sessions over V1 and MT. Pre-processing was computed in MATLAB, using the EEGLAB toolbox, the open source TMS-EEG Signal Analyser (TESA) plugin[84] and the Brainstorm plugin.[79]

Detection of bad channels was performed using the EEGLAB built-in function. Then, the raw EEG signal was epoched in a window of [-0.2, 0.8]s around the stimulation pulse onset, and demeaned. Afterwards, a window of [-5, 25]ms around the pulse onset was removed, to remove the TMS artefact, and the missing data was interpolated using a cubic function by considering the data 5ms before and after the removed TMS artefact window. EEG data were then down-sampled from 5000Hz to 1000Hz, and bad epochs (huge rubbing artefacts or undefined, significant noise) were removed by visual inspection. On average, 13 epochs out of 90 were removed per recording. Interpolated data in the TMS artefact window were removed gain, in order to compute the first round of Independent Component Analysis (ICA), aiming at eliminating components of the pulse artefact. This first ICA was computed by first performing a PCA compression using the TESA built-in function, and by then performing a symmetric fast-ICA with hyperbolic tangent as contrast function. The artefact components were removed manually by visual inspection. On average, 7 ($\pm$3) components out of 64 were removed. The EEG signal was re-interpolated in the removed window as described previously, and frequency filtered with a bandpass filter between 1 and 80Hz, with a 4th degree Butterworth notch filter between 48 and 52Hz to remove the power line noise. Data belonging to the artefact window were removed once more as described earlier, and a second round of fast-ICA was computed to remove other types of artefacts, such as eye movement, blinking, acoustic artefacts and small head movement.[84] On average, 4 ($\pm$1) components out of 64 were removed. Finally, the EEG signal was spatially filtered using a Common Average Reference (CAR) filter.

TMS-EEG local/remote source activity (L/RSA)

Source reconstruction for each TEP was performed following the default procedure proposed in the Brainstorm (version 23-Mar-2022) software[85] together with the OpenMEEG Boundary Element Method (BEM) plugins. First, to each individual was assigned a default head model (ICBM152), with cortex and head meshes (15,000 and 10,000 vertices respectively). The forward model was then computed using the symmetric BEM developed in the OpenMEEG freeware, using default values for conductivity and layer thickness.[86] The locations of the electrodes were individually co-registered on the head model. For each of the single pulse TMS selected epochs, the source level activation was computed using a minimum norm imaging linear method with sLORETA as the inverse model. The dipole orientation of the source model was defined as unconstrained to the cortex surface. Source orientation was kept orthogonal to the cortical surface and source amplitude was estimated using the default values of the Brainstorm implementation of the whitened and depth-weighted linear L2-minimum norm solution.

In order to extract local and remote source activity (L/RSA) power, two ROIs were created on each individual anatomy using the individual TMS coordinates for V1 and MT (see above, section "single pulse TMS"), covering about 195 vertices of cortical mesh for V1 and 320 for MT. LSA and RSA power was then computed for each cortical target by averaging the absolute, smoothed (using a spatial smoothing filter with full width at half maximum of 5 mm) and normalized (z-score against baseline) source activity within its corresponding ROI. LSA consisted in the matched condition where local source activity was extracted. RSA consisted in the same procedure but extracting source activity of the non-stimulated area (unmatched condition - see above figure). Grand average L/RSA power was finally calculated for each stimulation site and ccPAS condition by averaging L/RSA power across subjects. Note that LSA refers to the matched condition (source activity extracted locally) and RSA refers to the unmatched condition (source activity extracted from the other region). The focus of the study was on LSA and RSA early components (<200ms after the onset).

TMS-EEG connectivity analysis

We explored effective connectivity at different frequency ranges using spectral Granger Causality, which is a metric of directed interareal influence[53] in a broader visual network known to be involved in motion direction discrimination.[35] Local source activity was extracted from two areas in addition to V1 and MT: the inferior parietal sulcus (IPS, ~120 vertices) and the Frontal Eye Field (FEF, ~140 vertices).

Granger causality is a measure of linear dependence, which tests whether the variance of error for a linear auto-regressive (AR) model estimation of a signal *x(t)* can be reduced when adding a linear model estimation of a second signal *y(t)*. If this is true, signal *y(t)* has a Granger causal effect on the first signal *x(t)*, i.e., independent information of the past of *y(t)* improves the prediction of *x(t)* above and beyond the information contained in the past of *x(t)* alone. The term independent is emphasized because it creates some interesting properties for Granger Causality, such as that it is invariant under rescaling of the signals, as well as the addition of a multiple of *x(t)* to *y(t)*. The measure of Granger Causality is non-negative, and zero when there is no Granger causality. According to the original formulation of Granger Causality, the measure of Granger Causality from *y(t)* to *x(t)* is defined as:

$$F_{y\to x} = \ln\left(\frac{Var(e_1)}{Var(e_2)}\right)$$

Which is 0 for $Var(e_1) = Var(e_2)$ and a non-negative value for $Var(e_1) > Var(e_2)$. Note that $Var(e_1) \geq Var(e_2)$ always holds, as the model can only improve when adding new information. Under fairly general conditions, $F_{y\to x}$ can be decomposed by frequency if the two AR models in time domain are specified as:

$$\mathrm{x(t)} = \sum_{k=1}^{p}\left[A_{k_{xx}}x(t-k) + A_{k_{xy}}y(t-k)\right] + \sigma_{xy}$$

$$\mathrm{y(t)} = \sum_{k=1}^{p}\left[A_{k_{yy}}y(t-k) + A_{k_{yx}}y(t-k)\right] + \sigma_{yx}$$

In each equation the reduced model can be defined when each signal is an AR model of only its own past, with error terms σ_{xx} and σ_{yy}. We can then define the variance-covariance matrix of the whole system as:

$$\sum = \begin{bmatrix} \sum_{xx} & \sum_{xy} \\ \sum_{yx} & \sum_{yy} \end{bmatrix}$$

Where $\sum_{xx} = Var(\sigma_{xx})$, etc. Applying a Fourier transform to these equations, they can be expressed as:

$$\begin{pmatrix} A_{xx}(\omega) & A_{xy}(\omega) \\ A_{yx}(\omega) & A_{yy}(\omega) \end{pmatrix}\begin{pmatrix} x(\omega) \\ y(\omega) \end{pmatrix} = \begin{pmatrix} \varepsilon_1(\omega) \\ \varepsilon_2(\omega) \end{pmatrix}$$

Rewriting this as:

$$\begin{pmatrix} x(\omega) \\ y(\omega) \end{pmatrix} = \begin{pmatrix} H_{xx}(\omega) & H_{xy}(\omega) \\ H_{yx}(\omega) & H_{yy}(\omega) \end{pmatrix}\begin{pmatrix} \varepsilon_1(\omega) \\ \varepsilon_2(\omega) \end{pmatrix}$$

Where $H(\omega)$ is the transfer matrix, the spectral matrix is then defined as:

$$S(\omega) = H(\omega)\sum H^*(\omega)$$

Finally, assuming independence of the signals *x* and *y*, and $\sum_{xy} = \sum_{yx} = 0$, we can define the spectral Granger Causality as:

$$F_{y\to x}(\omega) = \ln\left(\frac{S_{xx}(\omega)}{H_{xx}(\omega)\sum_{xx}H^*_{xx}(\omega)}\right)$$

Granger Causality was then computed between the four clusters (V1, MT, IPS and FEF), in a frequency range of 1-45 Hz and with a definition of 3 Hz, in order to explore the role of different rhythms in the causal connectivity between brain regions. Note that the use of Granger causality on source-projected EEG data reduces the problem of signal mixing and volume conduction, probably because Granger causality reflects causal, i.e. time-delayed, interactions, and explicitly discards instantaneous interactions resulting from signal mixing.[38,39,87] Importantly, we computed Granger Causality on the EEG signals in response to single pulse TMS. This combination allowed us to distinguish direct output signals from re-entrant signals (see above figure). In the manuscript, we used the term "*output connectivity*" to refer to the condition where single-pulse TMS was applied to the first area (e.g., TMS over V1, Granger Causality from V1 to MT). In contrast, we refer to "*re-entrant connectivity*" for the condition when TMS was applied to the second area (e.g., TMS over MT and Granger Causality from V1 to MT).

QUANTIFICATION AND STATISTICAL ANALYSIS

Behavioural data

We computed direction range thresholds by fitting a Weibull function to the percentage correct performance at each stimulus level and computed the stimulus value (i.e., direction range), resulting in 75% correct performance. This criterion was selected because it lays halfway between chance (50% correct) and 100% correct on this two-alternative task (Huxlin et al., 2009). Direction range thresholds were then normalized by the maximum range (360) to produce the Normalized Direction Ratio (NDR) (e.g., Sailonz et al., 2010) using the following formula:

$$NDRthreshold(\%) = \left[\frac{(360^{\circ} - WeibullfittedDR)^{\circ}}{360}\right] * 100$$

NDR values were entered into a mixed ANOVA that included Time (Pre vs Post) and ccPAS type (Forward *versus* Backward) as within-subject factor and ccPAS order (first Forward *versus* first Backward) as between-subject factor. Post hoc t-tests were performed when appropriate and significance was defined for p values <0.05.

EEG data: Significant differences in L/RSA curves as well as in connectivity strength/frequency-resolved Granger Causality were evaluated within-subjects through a non-parametric, cluster-based, corrected, permutation testing, excluding frequency-wise outliers (>2SD).[88]

Behavior and EEG: Individual NDR values were then computed as a ratio expressing the change between pre- and post-tests, and entered into forward stepwise regressions to determine which neural pathway modulation(s) (V1-to-MT or MT-to-V1) and which frequencies best predicted changes in motion direction discrimination.